2018 IEEE Intelligent Vehicles Symposium (IV)
Changshu, Suzhou, China, June 26-30, 2018

Radar-Based Analysis of Pedestrian Micro-Doppler Signatures Using Motion Capture Sensors

Patrick Held[1], Dagmar Steinhauser[1], Alexander Kamann[1], Thomas Holdgrün[1], Igor Doric[1], Andreas Koch[2] and Thomas Brandmeier[1]

***Abstract*— For the realization of autonomous driving, early detection and classification of vulnerable road users such as pedestrians is indispensable. High-resolution radars in the short range enable the detection of pedestrian-identifying micro-Doppler distributions. Especially the limb motion can provide fundamental features, which can support the design of automotive safety systems. This paper presents a detailed analysis of high-resolution human micro-Doppler signatures in terms of their composition by characteristic limb movements using synchronized measurements of a motion capture system. The use of state-of-the-art radar sensor technology as well as signal processing including clustering and OS-CFAR filtering leads to comparisons of simultaneously captured movements with the associated micro-Doppler signatures and provides new insights in the detailed radar-based analysis of the human gait. The potential feasibility to detect characteristic features for predictive algorithms is discussed and analyzed on the basis of realistic automotive scenarios such as road crossing movements.**

I. Introduction

Recent advances in the development of 77 and 79 GHz technology allow the potential use of high-resolution radar sensors in the closer vehicle environment for detection and classification of vulnerable road users (VRU) like pedestrians. For this purpose, the micro-Doppler effect (μD) is used. An investigation of radar-based human μD signatures has been of high relevance for automotive safety applications, particularly with regard to autonomous driving. Consequently, there have been studies and researches on this topic [1]–[4], where basic classifications based on periodic μD patterns are achieved. The detailed analysis of individual velocity components of corresponding limbs during the human movement is still of particular interest. Since the radial Doppler frequencies of the human components are superimposed in the time-frequency domain and thus not satisfactorily assignable, data recorded by full body human motion capture (MoCap) sensors give a much more comprehensible movement behavior. The objective of this paper is to analyze measured μD signatures of the human gait with high range and velocity resolutions in different relevant scenarios for automotive pedestrian safety based on associated MoCap reference data.

[1]The authors are with the Center of Automotive Research on Integrated Safety Systems and Measurement Area (CARISSMA), Technische Hochschule Ingolstadt, Ingolstadt, Germany. Email: {patrick.held, dagmar.steinhauser, alexander.kamann, thomas.brandmeier}@carissma.eu

[2]Andreas Koch with Continental, Business Unit ADAS, Peter-Dornier-Straße 10, Lindau, Germany. Email: andreas.6.koch@continental-corporation.com

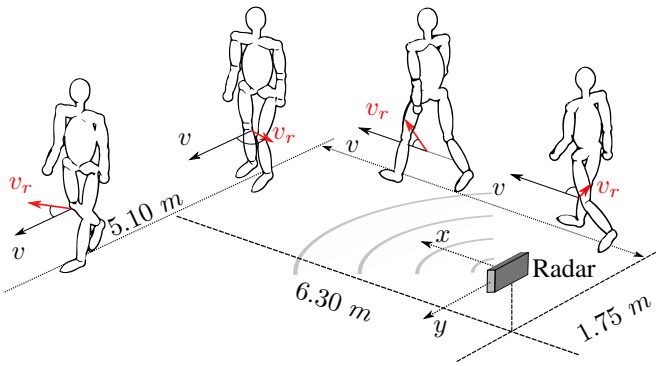

Fig. 1: Road crossing movement scenario.

II. Related Works

In the field of radar-based pedestrian detection several investigations use radar simulations based on MoCap data. In [5], Schubert et al. introduce a multi-reflection pedestrian model for automotive use. Through video recordings of marked subjects motion capture data are created, although due to the cinematic method only one body side can be measured continuously. The radial velocity components of the MoCap signals input a simulation framework, which returns μD signatures. The radar cross section (RCS) values of individual reflection points are percentage distributions corresponding to their body areas on the basis of an average total value from literature. In [6], Belgiovane et al. first use camera based MoCap data of a walking and running pedestrian to input a μD simulation. Afterwards they present measured μD signals of a radially and laterally walking pedestrian in the 77 GHz band for different sensor heights. Due to the asynchronous measurement of MoCap data and radar data, the assignment of the limbs by μD signals is based on unreferenced interpretations. In [7], first attempts to decompose human μD signals based on MoCap data are presented. The movement behavior of a marked subject is recorded by infrared cameras. However, the radar data are not measured. Instead they are created by a simulation in the 24 GHz band, which leads to significantly simplified radar returns, which are not comparable to measured data in terms of complexity. In [8], He et al. present an approach to extend the standard time-frequency representation of μD signals by the distance dimension. This approach indicates, that additional consideration of the range dimension could help to separate body parts when using high-resolution radars.

978-1-5386-4451-5/18/$31.00 ©2018 IEEE

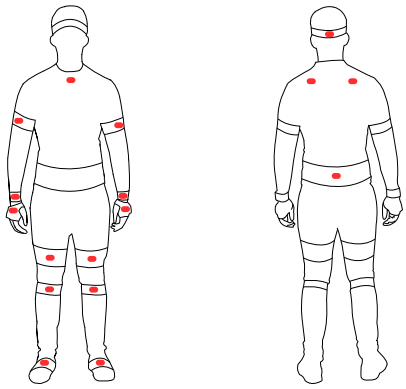

(a) (b)

Fig. 2: Subject wearing 17 acceleration sensors (red markings) in front and back view.

Separately measured radar data show some basic similar characteristics, but the paper presents no direct comparison with associated MoCap data.

In summary, there are some approaches analyzing the reconstruction of μD data of human movements. However, in most cases MoCap data are used to create radar simulations. They are not used as a reference to support the interpretation of measured μD signals. Due to the independence between the MoCap data and the measured radar data, characteristic details can not be referenced with the matching movement behavior. Furthermore, simulations of human μD signatures for the analysis of characteristic movements need to be considered carefully. Despite the fact, that μD simulations are able to reproduce characteristics, which can be detected in measured data, they are still simplified. In most cases, simulations are based on the consideration of individual reflection points. Thus, they do not take into account the velocity distribution that results from large reflecting surfaces, such as that of the leg. The assignments to certain limbs are usually based only on similarities between simulations and measurements. However, the missing consideration of all body parts in simulations can lead to erroneous identifications of body components. Additionally, radar measurements are exposed to disturbing influences such as noise or multipath reflections (e.g. on the ground), which are usually neglected in simulations. Therefore, the verification of algorithms on real data is crucial. The direct comparison of measured radar data and the associated MoCap reference of the same experiment is still missing and thus has not been analyzed yet. This paper enables the identification of individual body parts in the radar image and allows a more detailed understanding of the human μD-effect and the predictive behavior in highly relevant automotive scenarios. This paper is organized as follows. Section III introduces the experimental setup consisting of the used motion capturing system and the radar sensor and gives an overview of the selected trajectory scenarios. Section IV presents the chirp sequence modulation and provides the applied signal processing for the creation of the μD visualizations. In section V the measured μD signatures with the associated motion capture signals of different movement scenarios are presented and analyzed. Finally, Section VI summarizes the results and discusses future work.

TABLE I: Radar Configurations

Parameter	Value
Center frequency	77 GHz
Bandwidth	2 GHz
Range resolution	0.075 m
Sampling frequency	10 MHz
Chirp duration	52.5 μs
Samples per chirp	512
Number of chirps	1024
Chirp repetition interval	62.5 μs
Sensor height	0.65 m
Azimuth 3 dB beamwidth (TX)	51°
Azimuth 3 dB beamwidth (RX)	76.5°

III. Experimental Setup

A. Motion Capture System Setup

For the digital recording of the corresponding human movements the Xsens MTw Awinda wireless full body motion capture system is used. This MoCap system consists of an inertial measurement unit containing 3-D linear accelerometers and rate gyroscopes [9]. 17 trackers are attached to defined locations on the subjects body, as shown in Fig. 2, to measure the motion of each body segment. A total of 22 trackers are available, 17 are actual sensors, whereas 5 of them (vertebra L3, T8, T12 and left and right toe) are interpolated approximations based on the subjects body sizes. The communication between the sensors and the synchronization station takes place by radio every 16.6 ms.

B. Radar Setup

For radar measurements the INRAS Radarlog is used with a uniform linear array frontend of 2 transmit and 16 serial fed patch receive antennas. This radar platform allows transmitting linear frequency modulated continuous wave (FMCW) signals in the form of chirp sequence modulations in the 77 GHz band. The sensor provides an interface for raw data signal processing with MATLAB. The specifications for the used parameters are given in Table I.

C. Pedestrian Trajectories

In the first trajectory, the pedestrian walks radially towards the radar starting 15 m away from the sensor and stops 2 m before the sensor. The second trajectory is shown in Fig. 1 and represents a pedestrian crossing the street in front of the radar. The pedestrian firstly walks away from the sensor in a parallel movement to the street. Thereafter, the pedestrian crosses the street, which corresponds to a lateral movement considering the radar sensor.

IV. Signal Processing

A. Chirp Sequence Modulation

A chirp sequence radar transmits successive linear frequency modulated chirps of the form [10]–[12]

$$x_T(t) = \cos\left(2\pi\varphi_T(t)\right),\ \varphi_T(t) = f_0 t + \gamma t^2,\ t \in [0, T], \quad (1)$$

where f_0 is the carrier frequency, φ_T is the transmitting signal phase and $\gamma = B/2T$ defines the chirp's half slope with bandwidth B and chirp duration T. The backscattered signal reaches the receiver antennas with a time delay $\tau << T$ of

$$x_R(t) = \xi\cos(2\pi\varphi_R(t)), \quad \varphi_R(t) = \varphi_T(t-\tau). \quad (2)$$

ξ summarizes all the attenuations the signal experiences during the signal path and φ_R is the receiving signal phase. After a down conversion to the baseband followed by a low-pass filtering, the intermediate frequency (IF) signal of one chirp is given by

$$\begin{aligned} x_{\text{IF}}(t) &= \xi\cos(2\pi\varphi_{\text{IF}}(t)), \quad \varphi_{\text{IF}}(t) = \varphi_{\text{T}}(t) - \varphi_{\text{R}}(t), \quad (3)\\ \varphi_{\text{IF}}(t) &= f_0 t + \gamma t^2 - f_0(t-\tau) - \gamma(t-\tau)^2 \\ &= f_0\tau + 2\gamma\tau t - \gamma\tau^2. \end{aligned}$$

Assuming $\tau << T$, the last term $\varphi_{\text{IF}}(t)$ can be neglected. If a target in a distance R is moving with a constant relative velocity v, the travel time is $\tau = 2(R+vt)/c_0$. The IF phase is then

$$\varphi_{\text{IF}}(t) = \frac{2f_0R}{c_0} + \left(\frac{4\gamma R}{c_0} + \frac{2f_0v_r}{c_0}\right)t + \frac{4\gamma v_r}{c_0}t^2, \quad (4)$$

where c_0 is the speed of light and v_r is the radial component of v. The first term defines a constant phase. The second term contains the beat frequency, which consists of a frequency change caused by the distance and the Doppler shift deriving from the relative velocity of the target. The last term is the Range-Doppler-Coupling, which indicates the frequency change due to a distance change induced by the movement of the target within a coherent processing interval (CPI). In the following, this term is neglected [10]. For a series of L transmitted chirps (4) can be extended to

$$\varphi_{\text{IF}}(t_l, l) = \frac{2f_0R}{c_0} + \frac{2f_0v_rT_{\text{PRI}}l}{c_0} + \left(\frac{4\gamma R}{c_0} + \frac{2f_0v_r}{c_0}\right)t_l, \quad (5)$$

where T_{PRI} is the pulse repetition interval, which includes the chirp duration T and the duration of the down-chirp. In the case of several reflection objects, the IF signal x_{IF} consists of superimposed oscillations with different frequencies. The obtained signal can be seen as a 2-D signal, since it has two dependent time variables t_l and l. The time variable t is redefined as $t = T_{\text{PRI}} \cdot l + t_l$, where $t_l \in [0, T]$ is the duration of the l-th chirp, whereas $l \in [0, L-1]$ defines the time variable over all chirps within a CPI. Due to the steep chirp slope γ, the Doppler shift is much smaller than $(4\gamma R)/(c_0)$. Therefore the Doppler shift of one received chirp can be neglected. Thus, its beat frequency contains only the range information, which can be evaluated by a Fourier transform along the time t_l for each chirp l. However, a phase difference occurs from chirp to chirp, which is directly proportional to the target's radial velocitiy. By applying a second Fourier transform for every range gate over the L chirps of one CPI, the Doppler frequencies can be extracted.

B. Target Detection and Clustering

Performing the 2-D Fourier transform, a range-Doppler spectrum is created for each time step. The detection is performed using an ordered statistics constant false alarm rate (OS-CFAR) filter [13], which adaptively estimates the detection threshold of each range-Doppler-cell based on the neighboring cells. Due to the high resolution in range as well as velocity, a large number of detection points are obtained. They are generated by reflection at the pedestrian as well as at other present objects (e.g. walls). In order to separate the reflections of the pedestrian from other objects as well as noise, the detection points are clustered following the method of Density-Based Spatial Clustering of Applications with Noise (DBSCAN) [14]. A neighborhood is defined by a distance ϵ in which a minimum number of points are required to form a dense region. The ϵ value is set to 0.5 m in the range domain, whereas ϵ is set to 1.5 m/s in the velocity domain and the number of points is set to 5. The following results and interpretations are solely based on the consideration of the cluster belonging to the pedestrian.

C. Spectrograms

In the field of human motion analysis the μD-effect can be described as a time-varying Doppler frequency change in the time-frequency domain. This behavior is composed of the superposition of different frequency components caused by the periodically moving limbs by a walking human [15]. To visualize the μD signatures, a spectrogram is created. The spectrogram is a time-frequency distribution and can be viewed as the energetic version of the Short-time Fourier Transform ($STFT$) [16] defined as

$$SPEC(t,\omega) = |STFT(t,\omega)|^2. \quad (6)$$

The analytic formulation of the $STFT$ is given by

$$STFT(t,\omega) = \int_{-\infty}^{\infty} w(\tau)x(t+\tau)e^{-j\omega\tau}d\tau. \quad (7)$$

The $STFT$ represents the Fourier transform of a signal $x(t)$, convolved by a window function $w(\tau)$. In this case the signal $x(t)$ corresponds to $x_{\text{IF}}(l)$. As a window function, a Hann window with a window length of 512 samples is selected. By sliding this window over $x_{\text{IF}}(l)$ for each range gate, the Doppler frequencies are extracted. With a window length of 512 samples at 1024 chirps per CPI, a satisfactory tradeoff between frequency and time resolution is achieved.

V. Human μD Signatures

A. Radially moving pedestrian

In the following, the CFAR-filtered, clustered and range compensated spectrograms of the measured μD signals are visualized as time-velocity distributions and compared with

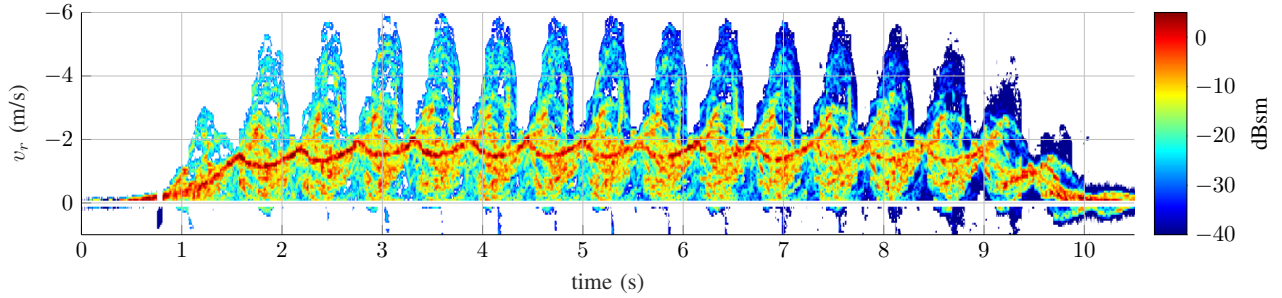

(a) Spectrogram of measured μD radar data.

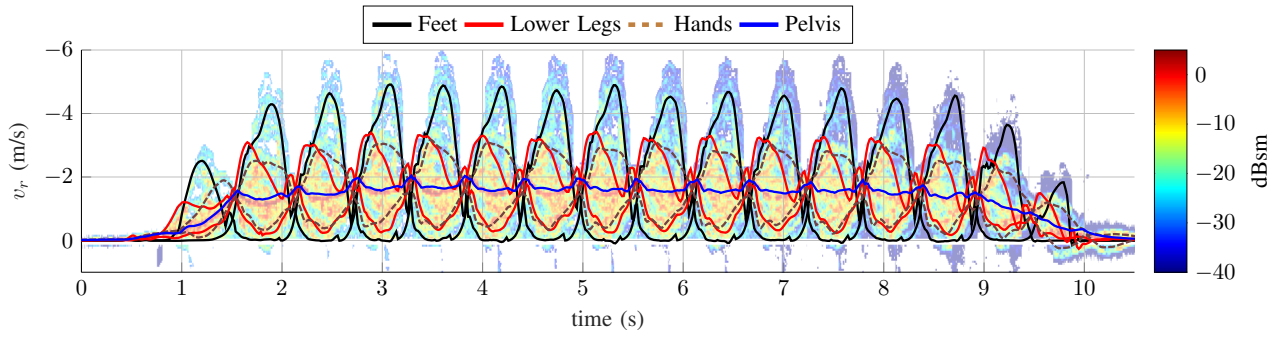

(b) Spectrogram of measured μD radar data with MoCap data of the feet, hands, lower legs and pelvis.

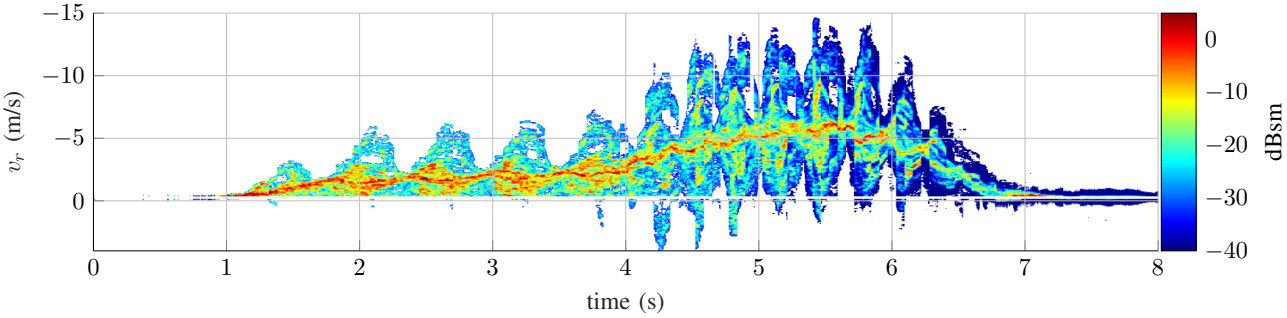

(c) Spectrogram of measured μD radar data.

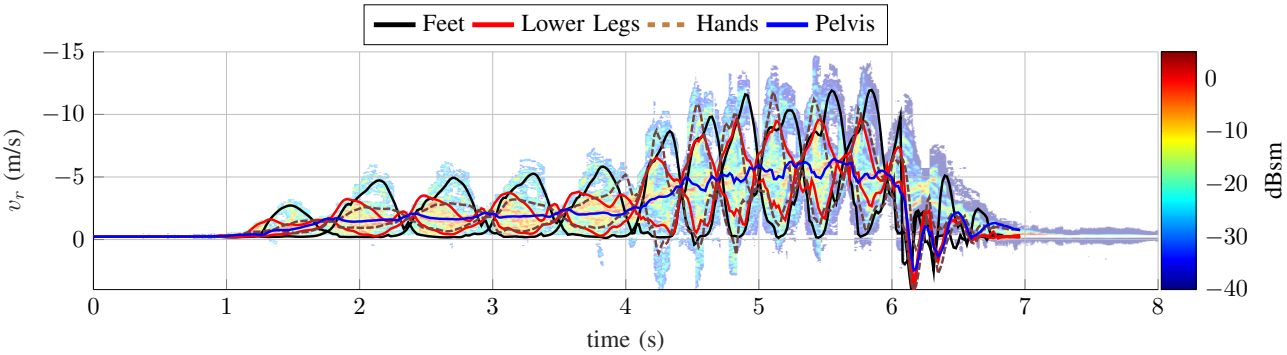

(d) Spectrogram of measured μD radar data with MoCap data of the feet, hands, lower legs and pelvis.

Fig. 3: Spectrograms and corresponding MoCap data of a radially towards the sensor walking/running pedestrian.

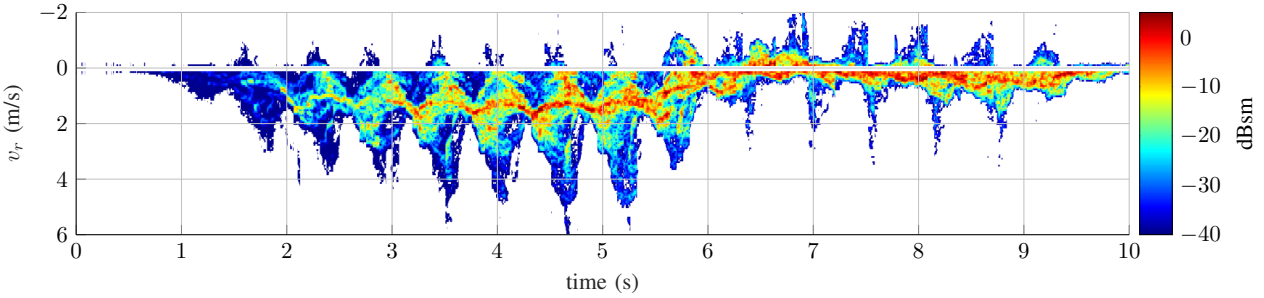

(a) Spectrogram of measured μD radar data.

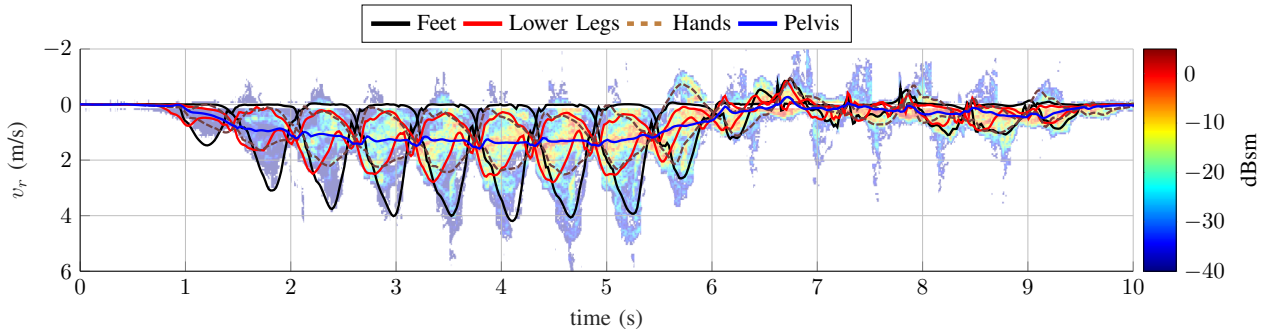

(b) Spectrogram of measured μD radar data with MoCap data of the feet, hands, lower legs and pelvis.

Fig. 4: Spectrograms and corresponding MoCap data of a pedestrian, who first moves parallel away from the sensor and then crosses laterally the radar's field of view.

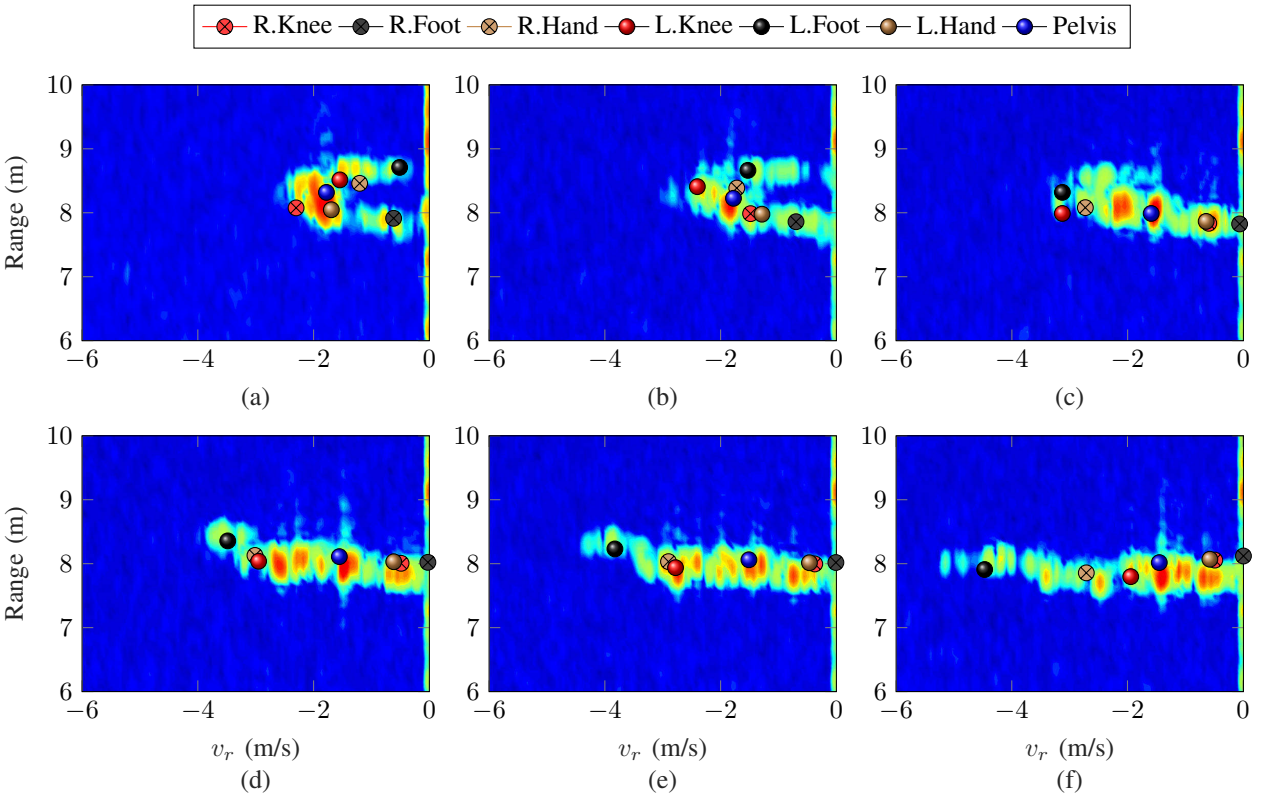

Fig. 5: Frame sequence of the range-velocity behavior of radar and MoCap data during a quarter gait cycle beginning with a stance phase, where the right foot is closer to the sensor.

the associated MoCap data. In order to enhance clarity, only selected characteristic body components of the MoCap data are shown. Those include the hands, the lower legs, the feet and the pelvis. The lower legs are more likely to be considered as the knee regions since the corresponding sensors have been attached directly below the knee joints (see Fig. 2(a)). Fig. 3(a) shows the measured radar results for a pedestrian walking radially towards the sensor. In addition, the corresponding velocity behavior of the selected limbs recorded by the MoCap sensors is depicted in Fig 3(b). This representation allows a better understanding of the radar image composition. The periodically changing velocity amplitude of the pedestrian is clearly visible due to the relatively high radial velocity components. As expected, MoCap data confirm, that the highest velocity components in the radar image are caused by the feet movement with values up to -6 m/s. It can be seen, that the MoCap amplitude of the feet does not reach the highest value of the radar data. In addition to occuring signal processing effects for extended target reflections, this can be explained with the position of the feet sensors. As shown in Fig. 2, the sensors are placed on top of the feet. Since the velocity distribution of the feet can be approximately described by a pendulum, it can be assumed, that the maximum velocity during a swing phase occurs at the bottom of the feet. The missing length between the position of the sensors and the bottom of the feet is the main reason for the different maximum velocities. The region of the torso represents the largest reflection surface of the body. Consequently, it shows the highest backscatter intensities with RCS values up to -5 dBsm. The pelvis, as a representative of the torso, shows a very similar velocity behavior with an average radial velocity of about -1.8 m/s. The decrease in torso intensity with increasing duration of the measurement is explained by the fact, that the subject leaves the field of view as the distance to the radar sensor becomes smaller. The velocity behavior of the arms and lower legs almost coincide with maximum values of about -3 m/s and minimum values of about -0.5 m/s. Those body components are slightly recognizable as well in the radar image due to their rather strong reflective intensities.

The results show the temporal movement delay of the beginning acceleration of the limbs. It can be seen, that the movement of the knee joint represents the initial movement of a gait cycle. Fig. 5 shows the image sequence of an incipient quarter gait cycle, from which the initial movement of the knee emerges. Both, the radar sequence and the corresponding MoCap data, are directly superimposed in range and velocity over consecutive frames. The starting frame shows a stance phase, in which both feet have contact to the ground, while the right foot is the front foot. With the instantaneous beginning of the following cycle the velocity increase of the knee joint can be captured. This can also be identified in the μD data in Fig. 3(a) as a slight protrusion of the envelope. The acceleration movement of the left knee is accompanied by an acceleration of the left foot. Only as the third accelerating movement the right hand contributes to the moving limbs. Finally, Fig. 5(c) illustrates how the left foot overtakes the left knee in terms of velocity. This detectable movement behavior of a starting gait cycle indicates, that for further investigations in terms of separability of single limbs, the consideration of the range information can be eminently useful.

Fig. 3(c) presents the results for a pedestrian, who first walks radially to the sensor and then suddenly starts to run towards the sensor and finally decelerates heavily at the end. This scenario is intended to visualize the changing radial velocity components of a person during the transition from walking to running. At about 4 s the subject begins to run abruptly out of the walking motion. It can be seen, that the motion initiating the running process is the increasing velocity of one hand. At this point in time, the subject begins to gain momentum with his hands, which is clearly recognizable in the μD signal. Despite of the acceleration of the hand, the occurrence in time needs to be emphasized. The acceleration takes place between the gait cycles and thus contrary to the previous rhythm. This behavior is an indicator for the changing movement of a pedestrian, which might be considered for predictive algorithms that detect emerging changes for automotive use. For the duration of running, in addition to an obvious increase in all velocity components up to -14 m/s, a significant velocity increase of the hands compared to the walking phase is observable. They now show a quadrupled velocity value of approximately 10 m/s and thus reach or even exceed the velocity values of the feet. Moreover, the duration of the stance phases, where one foot is on the ground, is shortened by about three quarters compared to the walking phase.

B. Road crossing pedestrian

In addition to radial movements, lateral movements are of particular relevance with regard to radar-based pedestrian detection in automotive scenarios. Due to the fact, that radar sensors can only measure radial velocities, lateral movement patterns are challenging. For this reason the results of a pedestrian leaving the sidewalk to cross the street are presented in the following. As seen in Fig. 1, the beginning trajectory is parallel to the x-axis of the radar sensor and then changes into a laterally crossing movement. Fig. 4 shows the corresponding μD and MoCap data of this scenario. It should be noted, that the subject walks approximately at the same speed both in the radial scenario and in the crossing scenario. At first the pedestrian walks gradually into the radar's field of view, which explains the less backscatter intensity of the first few seconds. With increasing distance of the pedestrian from the radar, the angle between the magnitude vector of the object velocity and the radial projection v_r becomes smaller as shown in Fig. 1. This can be recognized as an increase of the radial velocity components up to 5 m/s. Before the change of direction takes place, the subject decelerates his gait velocity to initiate the transition from parallel to lateral with its left foot at around 5.5 s. This leads to a reduction of the velocity components. The swing of the left hand and consequently the rotation of the upper body induces the turning movement. At this specific point in time, at around

5.7 s, the sign of the left hand's velocity changes, which is well detectable in the radar image. This behavior can be used for the design of predictive algorithms in terms of pedestrian protection since the changing sign of the hand's velocity can be considered as an upcoming change in the direction of movement (e.g. road crossing). Immediately with changing the direction of movement at around 6.0 s the radial Doppler components drop drastically and get a negative value, since now the radial velocity vector points in the opposite direction of the radar orientation. This abrupt drop in the pedestrian's radial velocity can serve as an indicator for a sudden movement change towards a lateral orientation. With proceeding movement, v_r becomes smaller until it reaches zero at passing the x-axis of the sensor at around 7.0 s. Subsequently, v_r increases again with changed sign.

VI. Conclusion

The presented research analyzed high-resolution radar μD signatures of the human gait. After an introduction of the experimental setup, suitable signal processing approaches have been developed for the generation of time-frequency distributions of a pedestrian. By simultaneously using MoCap sensors during the radar measurement, the matching reference of the movement behavior could be provided. This approach allowed new insights into the detailed analysis of human μD signals and the extraction of features, which may be used for future classification algorithms in the field of radar-based pedestrian protection. By the combination of range and doppler dimension data, an explicit reconstruction of the pedestrian movement behavior considering the motion of the individual limbs during the beginning of a cycle could be exposed. Particular attention was paid to realistic, highly relevant movement scenarios such as crossing a road or a sudden change of the pedestrian's velocity. The resulting rapidly changing radial velocity components and their effects on the reliable detection of pedestrians could be demonstrated. Thereby, significant characteristics for an early prediction of the movement behavior could be obtained. However, the results and characteristic features obtained, are based exclusively on the individual movement behavior of one subject and thus can not be generalized. For this reason, further investigations on the movement behavior of several subjects need to be carried out and analyzed for matching characteristics and the availability for safety algorithms.

Acknowledgment

The authors would like to thank the German Federal Ministry of Education and Research (BMBF) within the funding program Forschung an Fachhochschulen (contract number 13FH7I03IA) and the ADC Automotive Distance Control Systems GmbH (Continental AG) for their support.

References

[1] M. O. Padar, A. E. Ertan, and C. G. Candan, "Classification of human motion using radar micro-doppler signatures with hidden markov models," in *2016 IEEE Radar Conference (RadarConf)*, pp. 1–6, May 2016.

[2] M. Andres, K. Ishak, W. Menzel, and H.-L. Bloecher, "Extraction of micro-doppler signatures using automotive radar sensors," in *Journal of RF-Engineering and Telecommunications*, pp. 371–377, 2012.

[3] M. Heuer, A. Al-Hamadi, A. Rain, M. M. Meinecke, and H. Rohling, "Pedestrian tracking with occlusion using a 24 ghz automotive radar," in *15th International Radar Symposium (IRS)*, pp. 1–4, 2014.

[4] S. Heuel and H. Rohling, "Pedestrian recognition based on 24 ghz radar sensors," in *11th International Radar Symposium*, pp. 1–6, June 2010.

[5] E. Schubert, M. Kunert, A. Frischen, and W. Menzel, "A multi-reflection-point target model for classification of pedestrians by automotive radar," in *2014 11th European Radar Conference*, pp. 181–184, 2014.

[6] D. Belgiovane and C. C. Chen, "Micro-doppler characteristics of pedestrians and bicycles for automotive radar sensors at 77 ghz," in *2017 11th European Conference on Antennas and Propagation (EUCAP)*, pp. 2912–2916, 2017.

[7] S. Abdulatif, F. Aziz, B. Kleiner, and U. Schneider, "Real-time capable micro-doppler signature decomposition of walking human limbs," in *2017 IEEE Radar Conference (RadarConf)*, 2017.

[8] Y. He, P. Molchanov, T. Sakamoto, P. Aubry, F. L. Chevalier, and A. Yarovoy, "Range-doppler surface: a tool to analyse human target in ultra-wideband radar," *in IET Radar, Sonar Navigation*, vol. 9, no. 9, pp. 1240–1250, 2015.

[9] *Xsens MVN User Manual*. Enschede, The Netherlands, November 2017.

[10] V. Winkler, "Range doppler detection for automotive fmcw radars," in *2007 European Microwave Conference*, pp. 1445–1448, 2007.

[11] E. A. Costa and R. B. Chadwick, "Signal processing and range spreading in the fm-cw radar," National Oceanic and Atmospheric Administration Environmental Research Laboratories, May 1984.

[12] P. Heidenreich, *Antenna Array Processing: Autocalibration and Fast High-Resolution Methods for Automotive Radar*. PhD thesis, Technische Universitt Darmstadt, 2012.

[13] A. K. Ludloff, *Praxiswissen Radar und Radarsignalverarbeitung*. Vieweg+Teubner Verlag, 2 ed., 1998.

[14] M. Ester, H. Kriegel, J. Sander, and X. Xu, "A density-based algorithm for discovering clusters in large spatial databases with noise," in *Proc. of 2nd International Conference on Knowledge Discovery and Data Mining*, pp. 226–231, 1996.

[15] V. Chen, *The Micro-Doppler Effect in Radar*. Norwood, MA 02062 USA: Artech House, 2011.

[16] L. Stankovic, M. Dakovic, and T. Thayaparan, *Time-Frequency Signal Analysis with Applications*. Norwood, MA 02062 USA: Artech House, 2013.